JAMES | Journal of Advances in Modeling Earth Systems®

RESEARCH ARTICLE
10.1029/2022MS003177

On the Resolution of Triangular Meshes

S. Danilov[1,2]

[1]Alfred Wegener Institute, Helmholtz Centre for Polar and Marine Research, Bremerhaven, Germany, [2]Jacobs University, Bremen, Germany

Key Points:

- Geometrical resolution of an equilateral triangular mesh is defined by the height of its triangles
- Quadrilateral and triangular meshes with the same number of vertices have approximately the same resolution

Correspondence to:

S. Danilov,
sergey.danilov@awi.de

Citation:

Danilov, S. (2022). On the resolution of triangular meshes. *Journal of Advances in Modeling Earth Systems*, *14*, e2022MS003177. https://doi.org/10.1029/2022MS003177

Received 3 MAY 2022
Accepted 27 SEP 2022

Abstract It is generally agreed that the resolution of a regular quadrilateral mesh is the side length of quadrilateral cells. There is less agreement on the resolution of triangular meshes, exacerbated by the fact that the numbers of edges or cells on triangular meshes are approximately three or two times larger than that of vertices. However, the geometrical resolution of triangular meshes, that is, maximum wavenumbers or smallest wavelengths that can be represented on such meshes, is a well defined quantity, known from solid state physics. These wavenumbers are related to a smallest common mesh cell (primitive unit cell), and the set of mesh translations that map it into itself. They do not depend on whether discrete degrees of freedom are placed on vertices, cells or edges. For equilateral triangles the smallest wavelength equals twice the triangle height. Resolutions of quadrilateral and triangular meshes approximately agree if they have the same numbers of vertices.

Plain Language Summary Some models used in climate studies are formulated on triangular computational meshes. We discuss how to determine the smallest scales that are resolved on such meshes. They are referred to as a mesh resolution. The notion of mesh resolution is commonly used to relate climate model results simulated on different meshes.

1. Introduction

Several recent global ocean circulation models are formulated on unstructured triangular meshes (Danilov et al., 2017; Korn, 2017; Wang et al., 2014) or their dual, quasi-hexagonal meshes (Ringler et al., 2013). Unstructured-mesh models are also widely used in coastal applications (see, e.g., Androsov et al., 2019; Chen et al., 2003; Fringer et al., 2006; Zhang et al., 2016). Triangular and hexagonal meshes are also common in atmospheric modeling (see, e.g., Dubos et al., 2015; Gassmann, 2013; Kühnlein et al., 2019; Skamarock et al., 2012; Wan et al., 2013). A question often arises on how to compare their resolution to that of the models formulated on regular quadrilateral meshes. In contrast to quadrilateral meshes, the number of cells and the number of vertices differ by the factor of two on triangular meshes, which creates an ambiguity. For a mesh composed of equilateral triangles the side of triangle is $\sqrt{3}$ larger than the distance between the centers of triangles. Which of these two lengths is an analog of the cell side length of quadrilateral meshes in terms of resolution?

The concept of "resolution" discussed here is a geometrical one, that is, we are interested in the largest wavenumbers or smallest wavelengths that characterize discrete data on a given triangular (or hexagonal) mesh. The geometrical resolution should not be mixed with effective resolution which characterizes the scales where dynamics are not affected by dissipation and numerical errors (see, e.g., Skamarock, 2004; Soufflet et al., 2016). The effective resolution depends not only on the mesh, but also on the details of discretization (including the placement of discrete variables) and numerical algorithm. While one is finally interested in the effective resolution, its estimates are difficult (Soufflet et al., 2016) and require dedicated studies. Existing studies show that for finite-volume models the effective resolution is much coarser than the geometrical resolution (see, e.g., Skamarock, 2004; Soufflet et al., 2016). A rigorous definition of geometrical resolution in this work cannot compensate for the lack of dedicated studies on effective resolution for common finite-volume discretizations on triangular meshes. However, it reduces the ambiguity occurring when one tries to relate simulations on triangular and quadrilateral meshes, or to distinguish between eddy resolving and coarse meshes as suggested by Hallberg (2013).

In fact, the question on geometrical resolution is addressed in numerous textbooks on solid state physics (see e.g., Kosevich, 2005). This work only repeats the known answers as applied to modeling on triangular meshes.

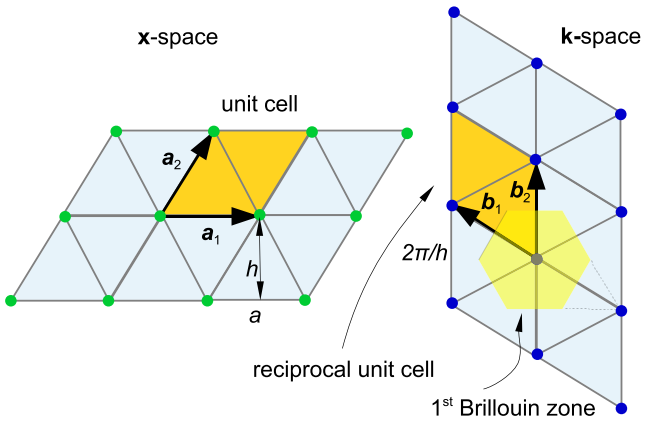

Figure 1. Triangular mesh, a unit cell, the reciprocal lattice and the first Brillouin zone. Left: Vectors $\mathbf{a}_1$ and $\mathbf{a}_2$ describe possible translation and define a unit cell of triangular mesh (the orange rhombus). Right: In $\mathbf{k}$-space, this leads to the set $\{\mathbf{q}_{r,s}\}$ of wavevectors (blue circles) creating a reciprocal lattice. A Voronoi cell of this lattice is the first Brillouin zone (the yellow hexagon). Wavevectors in reciprocal unit cell (orange rhombus) can be brought to the first Brillouin zone by translations $\mathbf{q}$. The triangle formed by dashed lines and the edge of hexagon, together with five similar triangles (not shown) form the second Brillouin zone.

The key concept is that of mesh translations that leave the mesh unchanged. They define a primitive unit cell (unit cell further), which is the smallest repeating element of the mesh. The invariance of mesh to these translations leads to a reciprocal lattice in wavenumber space, and wave vectors become defined up to translations along the reciprocal lattice. Section 2 introduces the notions of unit cell, reciprocal lattice, and the first Brillouin zone of triangular mesh. The first Brillouin zone defines the maximum resolved wavenumber. The same notions will be valid for dual Voronoi (hexagonal) meshes obtained by connecting circumcenters of triangles.

The area of unit cell turns out to be equal to that of median-dual control volume on triangular meshes or hexagonal cell on dual meshes, that is, the unit cells are directly related to vertex (cell) degrees of freedom (DOFs) of finite-volume discretizations on triangular (dual hexagonal) meshes.

The placement of discrete DOFs at vertices, cells or edges results in different numbers of discrete DOFs because the ratio of vertices to cells to edges is approximately 1:2:3 on triangular meshes and 2:1:3 on dual meshes. A naive expectation is that the resolved wavenumbers become larger if the DOFs are placed on cells or edges. This expectation lies behind such definitions of resolution as the square root of triangle area for cell placement of DOFs on triangular meshes, in analogy to quadrilateral meshes, where this is obviously the case. Sections 2 and 3 explain that the resolved wavenumbers and hence geometrical resolution for the cell and edge placement on triangular meshes are defined by the reciprocal lattice and are the same as for the vertex placement. Instead of larger wavenumbers, extra DOFs on cells or edges lead to the formation of numerical modes. Generally these modes are artifacts of discretizations. However, despite their presence and unchanged geometrical resolution, the cell or edge placement may ensure more accurate representation of physical mode, that is, a higher effective resolution, because of smaller numerical stencils.

The concluding section concentrates on practical aspects.

2. Resolved Wave Numbers

Resolved wave numbers are related to the smallest translationally invariant element of the mesh. Consider a regular infinite triangular mesh composed of equilateral triangles in plane geometry. We introduce coordinates x, y with origin at one of the mesh vertices and, for definiteness, orient the triangles so that all vertices are obtained through the set of translations $\mathbf{z} = \{\mathbf{z}_{m,n}\}$,

$$\mathbf{z}_{m,n} = m\mathbf{a}_1 + n\mathbf{a}_2, \quad \mathbf{a}_1 = (1,0)a, \ \mathbf{a}_2 = (1/2, \sqrt{3}/2)a, \tag{1}$$

where a is the triangle side length, and m, n are integer numbers. A rhombus, defined by vectors $\mathbf{a}_1$ and $\mathbf{a}_2$, is a unit cell of the triangular lattice (see Figure 1). The selection of vectors $\mathbf{a}_1$ and $\mathbf{a}_2$, and therefore the selection of rhombi is not unique, however all possibilities correspond to the same set of translations $\mathbf{z}$. Note that one needs to combine a pair of nearest triangles, one pointing upward/north and one pointing downward/south in the plane of Figure 1, to obtain a unit cell. Instead of this triangular mesh one may consider a dual mesh, obtained by connecting circumcenters of triangles with a common edge (the Voronoi tesselation). One deals with the same set of translations $\mathbf{z}$ in these cases.

Consider a Fourier harmonic $T = \overline{T}_{\mathbf{k}} e^{i\mathbf{k}\cdot\mathbf{x}}$ of scalar field T, where $\overline{T}_{\mathbf{k}}$ is the amplitude, $\mathbf{k} = (k, l)$ is the wave vector, and $\mathbf{x}$ the position vector. For simplicity, we sample this field at vertices of triangular mesh. The values of this field at the vertices $\mathbf{x}_{m,n} = \mathbf{z}_{m,n}$ will be the same if $\mathbf{k}$ is replaced by $\mathbf{k} + \mathbf{q}$, where $\mathbf{q}$ is such that

$$e^{i\mathbf{q}\cdot\mathbf{z}} = 1.$$

As a consequence, if the vertex values of T are used to find the wave vector $\mathbf{k}$, this can be done only up to vectors $\mathbf{q}$. The equation above implies that $\mathbf{q}$ is a set of wave vectors $\{\mathbf{q}_{r,s}\}$ in the wavenumber space,

$$\mathbf{q}_{r,s} = r\mathbf{b}_1 + s\mathbf{b}_2, \tag{2}$$

where r and s are integer numbers and the vectors $\mathbf{b}_1$ and $\mathbf{b}_2$ are such that

$$\mathbf{a}_i \cdot \mathbf{b}_j = 2\pi\delta_{ij},$$

which gives

$$\mathbf{b}_1 = (2\pi/a)(-1, 1/\sqrt{3}), \quad \mathbf{b}_2 = (2\pi/a)(0, 2/\sqrt{3}).$$

here, δ_{ij} is the Kronnecker delta, and $i, j = 1, 2$. The lattice formed by the points $\mathbf{q}_{r,s}$ is called *a reciprocal lattice* (Figure 1). A unit cell of the reciprocal lattice is a rhombus formed by $\mathbf{b}_1$ and $\mathbf{b}_2$ (painted orange in the right panel of Figure 1). Same as with the physical space, the unit cell is not uniquely defined, however all possibilities correspond to the same reciprocal lattice.

Because the wave vector $\mathbf{k}$ is defined up to $\mathbf{q}_{r,s}$, it is sufficient to consider $\mathbf{k}$ only within a unit reciprocal cell containing $\mathbf{q}_{0,0}$. However, a rhombic unit cell does not include all directions of wave vector, and is not suited to answer the question on geometrical resolution. One needs a set of $\mathbf{k}$-points that are closer to $\mathbf{q}_{0,0}$ than to any other $\mathbf{q}_{r,s}$. A polygon bounding this set is the Voronoi cell around $\mathbf{q}_{0,0}$. The cell is referred to as the first Brillouin zone of the reciprocal lattice. It is colored yellow in Figure 1. The wave vectors in the unit cell (orange) and in the first Brillouin zone (yellow) either coincide or differ by a wave vector from $\mathbf{q}$ and are indistinguishable on the triangular mesh. The first Brillouin zone contains wavenumbers that are closer to $\mathbf{q}_{0,0}$ than to any other $\mathbf{q}_{r,s}$ and thus defines maximum resolvable wavenumber. The Voronoi tesselation is produced by drawing lines perpendicular to the edges of triangular mesh through the edge midpoints. These lines also bound triangles lying outside the first Brillouin zone adjacent to its edges (one is shown by dashed lines in Figure 1). These triangles cover the first Brillouin zone if displaced by appropriately chosen $\mathbf{q}_{r,s}$. Taken together, they are referred to as the second Brillouin zone.

The longest wavevector bounded by the first Brillouin zone depends on the direction (see Figure 1). The worst case corresponds to the directions of vector $\mathbf{b}_1$ or $\mathbf{b}_2$:

$$|\mathbf{k}|_{\max} = |\mathbf{b}_1|/2 = 2\pi/(\sqrt{3}a) = \pi/h,$$

that is, the *geometrical* resolution of equilateral triangular mesh is defined by the height of triangles h. The resolution is higher in the direction of $\mathbf{a}_1$, but one is using the radius of the inscribed circle assuming isotropy.

At this point it is instructive to apply the same reasoning to a quadrilateral mesh with a cell side a. We obviously have $\mathbf{a}_1 = (1, 0)a$, $\mathbf{a}_2 = (0, 1)a$, and $\mathbf{b}_1 = 2\pi(1, 0)/a$, $\mathbf{b}_2 = 2\pi(0, 1)/a$, and conclude after drawing the Voronoi cell around $\mathbf{q}_{0,0}$ that the worst case is $|\mathbf{k}|_{\max} = \pi/a$. This is what is commonly referred to as the maximum wavenumber on a quadrilateral mesh.

On a regular triangular mesh obtained by splitting quadrilateral cells in two triangles, one will continue to deal with two lattice vectors, the unit cells and reciprocal lattice of the quadrilateral mesh. The maximum wavenumber will be π/a, same as for the quadrilateral mesh. Although we do not do it here, one can easily generalize computations to arbitrary regular triangular meshes.

The geometrical resolution is defined by the reciprocal lattice, which in turn is defined by the set of translations $\mathbf{z}$. The latter does not depend on the placement of discrete DOFs unless the placement and discretization formally corresponds to a finer mesh. (For example, placing DOFs at vertices and mid-edges and treating all these DOFs similarly corresponds to a finer mesh obtained by splitting each triangle in four by connecting mid-edges.) As a result, the geometrical resolution is independent of the placement of DOFs if $\mathbf{z}$ is not redefined.

3. What Happens if DOFs Are Placed on Triangles

There are more cells (triangles) and edges than vertices on triangular meshes, and the statement at the end of the previous section is counterintuitive. The intention of this section is to explain what happens using an example of cell placement.

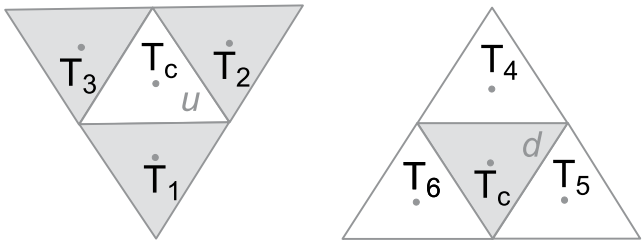

Figure 2. The stencils of neighbors of u and d triangles are oriented differently, leading to different discrete differential operators.

Figure 2 shows the nearest neighborhood of triangles pointing upward (u triangles) and downward (d triangles) in the plane of Figure 2. Because of the difference in the orientation of the stencil of neighbors, all discrete operators depend on whether they are computed on u or d locations. For definiteness, we consider the Laplacian of scalar field T given at cell locations.

For an equilateral triangular mesh the discrete Laplacian operator defined on the stencil of nearest neighbors is written as

$$(\mathsf{L}T)_c = \frac{4}{a^2} \sum_{n \in \mathcal{N}(c)} (T_n - T_c),$$

where $\mathcal{N}(c)$ is the set of (three) triangles neighboring triangle c (sharing edges). For Figure 2, $(\mathsf{L}T)^u_c = \left(4/a^2\right)(T_1 + T_2 + T_3 - 3T_c)$ for the left panel, and $(\mathsf{L}T)^d_c = \left(4/a^2\right)(T_4 + T_5 + T_6 - 3T_c)$ for the right panel. It can be readily shown that the expression for the Fourier symbol of L depends on the kind of triangle.

Indeed, let us take T as a single Fourier harmonic $T = \overline{T}_{\mathbf{k}} e^{i\mathbf{k}\cdot\mathbf{x}}$. Inserting this expression in the expressions for the Laplacian, we find

$$(\mathsf{L}T)^u_c = \left(4/a^2\right)\left(-3\bar{T}_{\mathbf{k}} + V\bar{T}_{\mathbf{k}}\right) e^{i\mathbf{k}\cdot\mathbf{x}_c}, \tag{3}$$

$$(\mathsf{L}T)^d_c = \left(4/a^2\right)\left(-3\bar{T}_{\mathbf{k}} + V^*\bar{T}_{\mathbf{k}}\right) e^{i\mathbf{k}\cdot\mathbf{x}_c}, \tag{4}$$

where $V = e^{-2ilh/3} + e^{-ika/2 + ilh/3} + e^{ika/2 + ilh/3}$ and the asterisk denotes complex conjugate. The exponents appearing in V take into account the phase differences between triangle c and its neighbors.

In the expressions for the Laplacian Equations 3 and 4 we factored out the phase multiplier $e^{i\mathbf{k}\cdot\mathbf{x}_c}$. This would have ensured that the amplitude of the Laplacian is independent of location if we were performing similar computations for quadrilateral cells. However, the complex-valued amplitudes of the Laplacian operator in Equation 3 and 4 differ at u and d locations because V is complex-valued, so that $V \neq V^*$. This means that the field of Laplacian due to a single Fourier harmonic is double-valued if we factor out the phase multiplier $e^{i\mathbf{k}\cdot\mathbf{x}_c}$: the result depends on whether it is assessed on u or d triangles. We would have arrived at the same conclusion using Taylor's series expansion of the discrete operators at u and d triangles or considering other differential operators.

As a consequence of this behavior, any evolving discrete field T defined on triangles will contain a mode of variability between u and d triangles. An analog of single Fourier harmonic in this case is the pair

$$T^u_c = \overline{T}^u_{\mathbf{k}} e^{i\mathbf{k}\cdot\mathbf{x}_c}, \quad c \in C^u,$$

$$T^d_c = \overline{T}^d_{\mathbf{k}} e^{i\mathbf{k}\cdot\mathbf{x}_c}, \quad c \in C^d,$$

where C^u and C^d are the subsets of triangles with the same orientation and $\overline{T}^u_{\mathbf{k}}$ and $\overline{T}^d_{\mathbf{k}}$ are respective amplitudes. Now note that in the computations of the Laplacian above, the result on a u location depends on the neighboring values of T on d locations and vice versa.

Thus, the Fourier symbol is the matrix

$$\mathsf{L}_{\mathbf{k}} = \left(4/a^2\right)\begin{pmatrix} -3 & V \\ V^* & -3 \end{pmatrix}.$$

It connects the amplitudes of Laplacian operator at u and d locations with the amplitudes of Fourier harmonic,

$$\begin{pmatrix} \overline{(\mathsf{L}T)}^u_{\mathbf{k}} \\ \overline{(\mathsf{L}T)}^d_{\mathbf{k}} \end{pmatrix} = \mathsf{L}_{\mathbf{k}} \begin{pmatrix} \overline{T}^u_{\mathbf{k}} \\ \overline{T}^d_{\mathbf{k}} \end{pmatrix}.$$

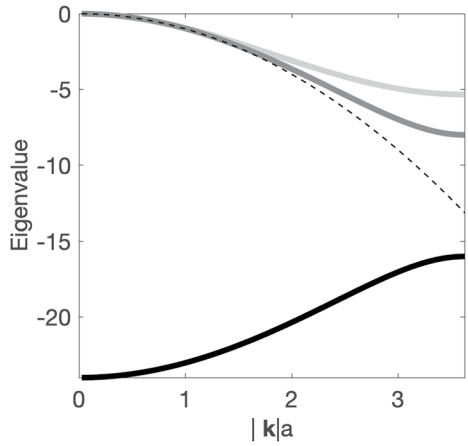

Figure 3. The dimensionless eigenvalues $a^2\lambda$ (light gray, vertex placement), and $a^2\lambda_+$ and $a^2\lambda_-$ (dark gray and solid black respectively, cell placement) of discrete Laplacians. **k** is directed at the angle of $\pi/6$ to the x-axis. The dashed line plots the continuous case $-a^2(k^2 + l^2)$. There is a gap between λ_+ (dark gray) and λ_- (black) at the boundary of the Brillouin zone $|\mathbf{k}|a = 2\pi/\sqrt{3}$. Since λ_- is disconnected from λ_+, it corresponds to the numerical mode of cell placement.

The eigenvalues of $\mathsf{L}_\mathbf{k}$ are

$$\lambda_\pm = (4/a^2)\left(-3 \pm \sqrt{VV^*}\right), \tag{5}$$

with the eigenvectors $\mathbf{v}_+ = \left(\sqrt{V}, \sqrt{V^*}\right)^T$ and $\mathbf{v}_- = \left(\sqrt{V}, -\sqrt{V^*}\right)^T$. One readily finds that λ_+ tends to $-k^2 - l^2$ if $ka, lh \to 0$, that is, it approximates the Fourier symbol of the continuous Laplacian operator. The other eigenvalue tends to $-24/a^2$; it does not provide an approximation. The first eigenvector tends to $\mathbf{v}_+ \to (1,1)^T$ for small wavenumbers. In contrast, $\mathbf{v}_- \to (1,-1)^T = \left(1, e^{i\pi}\right)^T$ for small wavenumbers, that is, it corresponds to a checkerboard pattern (oscillations within unit cells). This pattern is generally well controlled in numerical applications.

One can readily see that $\lambda_+ \neq \lambda_-$ at the boundary of the first Brillouin zone (except for the corners), as illustrated in Figure 3 (the dark gray and black lines). Because of this gap, λ_- cannot be a mapping from the second Brillouin zone to the first one and is a numerical mode. (If λ_+ and λ_- and the related eigenvectors were coinciding at the boundary of the first Brillouin zone, the distinction between u and d amplitude would be redundant.)

Thus by placing DOFs on cells instead of vertices (and doubling the number of discrete DOFs) one does not make the geometrical resolution finer, but creates a numerical mode in addition to the physical one. The edge placement would lead to similar consequences. Discretizations of primitive equations involve many additional details which are not considered here. The cell or edge placement of DOFs is used in finite-volume models based on staggered discretizations. For all them the geometrical resolution is determined by the sets of translations **z** and **q** in the **x**- and **k**-space respectively, same as for the collocated discretization by Kühnlein et al. (2019).

There are two related questions. First, if one is loosing DOFs to numerical modes for cell or edge placement, what does one gain using discretizations relying on cell or edge placement on triangular meshes? Second, what happens if one opts for high-order discretizations, for example, based on high-order continuous or discontinuous Galerkin methods. Such discretizations associate many discrete DOFs with each mesh element, and an expectation is that they would resolve larger wavenumbers.

The answer to the first question is that despite losing DOFs to numerical modes, one may get a more accurate physical mode than with the discretizations using the vertex placement. In addition to expected differences between staggered and collocated discretizations one more reason is that numerical stencils for differential operators imply smaller distances between the DOFs in such cases. Staying in the context of the example considered in this section, Figure 3 compares the eigenvalues of the discrete Laplacian for the cell-based DOFs Equation 5 with that of vertex discretization. The nearest-neighbor Laplacian in this case is approximated as

$$(\mathsf{L}T)_v = \left(1/2h^2\right)\left(-6T_v + \sum_{n\in\mathcal{N}(v)} T_n\right),$$

where v is the vertex index, and $\mathcal{N}(v)$ is the set of vertices neighboring v. Its Fourier symbol is $\lambda = (1/2h^2)(2\cos(ka) + 2\cos(ka/2 + lh) + 2\cos(-ka/2 + lh) - 6)$. Despite $(\mathsf{L}T)_v$ relies on more discrete values, the eigenvalue for vertex placement (light gray curve) is less accurate than λ_+ (dark gray curve).

It is therefore the effective resolution, and not the geometrical resolution that might be improved by using cell or edge placement provided that numerical modes are controlled. The example above is just an illustration that the effective resolution is affected by the placement of DOFs. We will not discuss this topic any further; it requires special studies and an account for numerous additional details (see, e.g., Soufflet et al., 2016). For some further details on discretizations and numerical modes see, for example, Le Roux (2012) and Danilov and Kutsenko (2019) and references therein.

Only a sketch of the answer is provided for the second question. Extra DOFs inside mesh unit cells will generally lead to additional modes of variability unless the discretization formally implies a smaller unit cells. However, for higher-order discretizations, the gaps between some of the modal eigenvalues at the boundary of the first Brillouin zone might become small. Such additional modes would become close to higher-wavenumber contributions from higher Brillouin zones into the first Brillouin zone (see, e.g., Cotter & Ham, 2011). They may imply subcell resolution if they are accurate enough. The question is whether (or when) the presence of gaps can be ignored. It requires further studies for particular cases.

4. Conclusions

The geometrical resolution of triangular meshes is rigorously defined by the size of the first Brillouin zone and corresponds to the wavenumber π/h, where h is the triangle height, for meshes based on equilateral triangles. It corresponds to π/a for meshes obtained by splitting quadrilateral cells with side a in a regular way. Thus h or a, respectively, have to be compared to the size of quadrilateral cells on regular quadrilateral meshes. Since triangles on meshes used in practice commonly tend to equilateral, we provide some further detail assuming that we deal with such meshes. The discussion will also be relevant for dual (hexagonal) meshes, in which case a is the distance between cell centers. Note that the analysis of Section 2 can be applied to arbitrary regular meshes.

Given quadrilateral and triangular meshes with the cell side a, the maximum wavenumber for an equilateral triangular mesh is $2/\sqrt{3}$ times higher than on the quadrilateral mesh. If S is the area of the computational domain, it will be covered by $N_q = S/a^2$ quadrilateral cells and $N_t = (2/\sqrt{3})S/a^2$ unit cells of triangular mesh. For $N_t = N_q$, a triangular mesh provides $(2/\sqrt{3})^{1/2}$ better resolution (about 9%) than its quadrilateral counterpart. The reason is a higher mesh symmetry. Thus, quadrilateral and triangular meshes are approximately equivalent in terms of geometrical resolution if they have close numbers of vertices, not cells (but cells have to be used to compare hexagonal and quadrilateral meshes). It is customary to characterize the size of computational triangular meshes by the number of vertices. For orientation, a typical 1/4° quadrilateral ocean mesh contains about 1M wet vertices, and there are about 9M wet vertices on a 1/12° quadrilateral mesh.

If a triangle side (or the distance between cell centers on dual meshes) is used to estimate the resolution, the estimate is too conservative, because $a \approx 1.16h$ for equilateral triangles. On the other hand, if the square root of triangle area is used as a measure of resolution for a discretization placing DOFs on cells, it gives the estimate $3^{-1/4}h \approx 0.75h$ which is 25% finer than the real resolution. The discrepancy becomes even worse if the distance between triangle centers is taken $(2h/3)$. A rather good estimate is provided by the square root of the area of unit cell (twice the triangle area or area of the dual cell) which is only 9% coarser than the real resolution. While each of such estimates can be acceptable under certain circumstances, they can be misleading in a general case when triangular meshes are compared to quadrilateral meshes. For example, with the definition of resolution as a square root of triangle area, a triangular mesh with triangle side 15.2 km (and height 13 km) is characterized as a 10 km mesh. The computational effort needed to run simulations on a quadrilateral meshes with nominal resolutions of 10, 13, or 15.2 km is quite different.

Although the notion of geometrical resolution could help to distinguish between coarse, eddy-permitting or eddy resolving meshes (see, e.g., Hallberg, 2013), and to approximately relate simulations carried out on meshes of different type (quadrilateral, triangular or hexagonal), it cannot be interpreted as a measure of real, effective resolution. For low-order discretizations as in the models mentioned in the Introduction, the effective resolution is much coarser than the geometrical one (Soufflet et al. (2016) report wavelengths of $10a$ against $2a$, where a is the cell side). Soufflet et al. (2016) demonstrate that the effective resolution is sensitive to many details of discretization, including time stepping and the order of advection schemes. Models formulated on triangular or hexagonal meshes come with additional factors like numerical modes and obviously different ratios between scalar and vector DOFs than on quadrilateral meshes. The central question for future research is on the effective resolution of the components of climate models formulated on triangular or hexagonal meshes.

Data Availability Statement

Data were not used, nor created for this research.

Acknowledgments
This work is a contribution to project S2 of the Collaborative Research Centre TRR181 "Energy Transfer in Atmosphere and Ocean" funded by the Deutsche Forschungsgemeinschaft (DFG, German Research Foundation) - Projektnummer 274762653. Open Access funding enabled and organized by Projekt DEAL.

References

Androsov, A., Fofonova, V., Kuznetsov, I., Danilov, S., Rakowsky, N., Harig, S., et al. (2019). FESOM-C v.2: Coastal dynamics on hybrid unstructured meshes. *Geoscientific Model Development*, *12*(3), 1009–1028. https://doi.org/10.5194/gmd-12-1009-2019

Chen, C., Liu, H., & Beardsley, R. C. (2003). An unstructured, finite volume, three-dimensional, primitive equation ocean model: Application to coastal ocean and estuaries. *Journal of Atmospheric and Oceanic Technology*, *20*(1), 159–186. https://doi.org/10.1175/1520-0426(2003)020<0159:augfvt>2.0.co;2

Cotter, C., & Ham, D. (2011). Numerical wave propagation for the triangular p1DG − p2 finite element pair. *Journal of Computational Physics*, *230*(8), 2806–2820. https://doi.org/10.1016/j.jcp.2010.12.024

Danilov, S., & Kutsenko, A. (2019). On the geometric origin of spurious waves in finite-volume discretizations of shallow water equations on triangular meshes. *Journal of Computational Physics*, *398*, 108891. https://doi.org/10.1016/j.jcp.2019.108891

Danilov, S., Sidorenko, D., Wang, Q., & Jung, T. (2017). The finite-volumE sea ice–ocean model (FESOM2). *Geoscientific Model Development*, *10*(2), 765–789. https://doi.org/10.5194/gmd-10-765-2017

Dubos, T., Dubey, S., Tort, M., Mittal, R., Meurdesoif, Y., & Hourdin, F. (2015). DYNAMICO-1.0, an icosahedral hydrostatic dynamical core designed for consistency and versatility. *Geoscientific Model Development*, *8*(10), 3131–3150. https://doi.org/10.5194/gmd-8-3131-2015

Fringer, O. B., Gerritsen, M., & Street, R. L. (2006). An unstructured-grid, finite-volume, nonhydrostatic, parallel coastal ocean simulator. *Ocean Modelling*, *14*(3–4), 139–173. https://doi.org/10.1016/j.ocemod.2006.03.006

Gassmann, A. (2013). A global hexagonal C-grid non-hydrostatic dynamical core (ICON-IAP) designed for energetic consistency. *Quarterly Journal of the Royal Meteorological Society*, *139*(670), 152–175. https://doi.org/10.1002/qj.1960

Hallberg, R. (2013). Using a resolution function to regulate parameterizations of oceanic mesoscale eddy effects. *Ocean Modelling*, *72*, 92–103. https://doi.org/10.1016/j.ocemod.2013.08.007

Korn, P. (2017). Formulation of an unstructured grid model for global ocean dynamics. *Journal of Computational Physics*, *339*, 525–552. https://doi.org/10.1016/j.jcp.2017.03.009

Kosevich, A. M. (2005). *The crystal lattice. Phonons, solitons, dislocations, superlattices*. WILEY-VCH Verlag.

Kühnlein, C., Deconinck, W., Klein, R., Malardel, S., Piotrowski, Z. P., Smolarkiewicz, P. K., et al. (2019). FVM 1.0: A nonhydrostatic finite-volume dynamical core for the IFS. *Geoscientific Model Development*, *12*(2), 651–676. https://doi.org/10.5194/gmd-12-651-2019

Le Roux, D. Y. (2012). Spurious inertial oscillations in shallow-water models. *Journal of Computational Physics*, *231*(24), 7959–7987. https://doi.org/10.1016/j.jcp.2012.04.052

Ringler, T., Petersen, M., Higdon, R., Jacobsen, D., Maltrud, M., & Jones, P. (2013). A multi-resolution approach to global ocean modelling. *Ocean Modelling*, *69*, 211–232. https://doi.org/10.1016/j.ocemod.2013.04.010

Skamarock, W. (2004). Evaluating mesoscale NWP models using kinetic energy spectra. *Monthly Weather Review*, *132*(12), 3019–3032. https://doi.org/10.1175/mwr2830.1

Skamarock, W., Klemp, J., Duda, M., Fowler, L., Park, S., & Ringler, T. D. (2012). A multiscale nonhydrostatic atmospheric model using centroidal Voronoi tesselations and C-grid staggering. *Monthly Weather Review*, *140*(9), 3090–3105. https://doi.org/10.1175/MWR-D-11-00215.1

Soufflet, Y., Marchesiello, P., Lemarié, F., Jouanno, J., Capet, X., Debreu, L., & Benshila, R. (2016). On effective resolution in ocean models. *Ocean Modelling*, *98*, 36–50. https://doi.org/10.1016/j.ocemod.2015.12.004

Wan, H., Giorgetta, M., Zängl, G., Restelli, M., Majewski, D., Bonaventura, L., et al. (2013). The ICON-1.2 hydrostatic atmospheric dynamical core on triangular grids –Part 1: Formulation and performance of the baseline version. *Geoscientific Model Development*, *6*(3), 735–763. https://doi.org/10.5194/gmd-6-735-2013

Wang, Q., Danilov, S., Sidorenko, D., Timmermann, R., Wekerle, C., Wang, X., et al. (2014). The finite element sea ice-ocean model (FESOM) v. 1.4: Formulation of an ocean general circulation model. *Geoscientific Model Development*, *7*(2), 663–693. https://doi.org/10.5194/gmd-7-663-2014

Zhang, Y. J., Ye, F., Stanev, E. V., & Grashorn, S. (2016). Seamless cross-scale modeling with SCHISM. *Ocean Modelling*, *102*, 64–81. https://doi.org/10.1016/j.ocemod.2016.05.002